Food and Bioprocess Technology
https://doi.org/10.1007/s11947-019-02384-x

ORIGINAL PAPER

Effect of Carboxymethyl Chitosan Magnetic Nanoparticles Plus Herring Antifreeze Protein on Conformation and Oxidation of Myofibrillar Protein From Red Sea Bream (*Pagrosomus major*) After Freeze-Thaw Treatment

Luyun Cai[1,2] · Linyu Nian[3,4] · Ailing Cao[5] · Yuhao Zhang[6] · Xiuxia Li[4]

Received: 27 August 2018 / Accepted: 28 November 2019

Abstract

The effects on the quality of frozen red sea bream, which were pretreated by soaking in solutions containing trehalose, carboxymethyl chitosan magnetic nanoparticles (CCMN), and glycerin or 0.1% herring antifreeze protein (hAFP), were investigated. In this study, the viscoelastic properties of protein studied with the dynamic rheology, Raman and intrinsic fluorescence spectrometry were used to explore the conformation changes of MFP. Surface hydrophobicity, particle size, and zeta potential were carried out to analyze protein aggregation. Solubility, the content of total sulfhydryl/disulfide bond/carbonyl/dityrosine, and the Ca^{2+}-ATPase activity were measured to explore the degree of protein oxidation. SDS-PAGE was conducted to analyze the protein denaturation. Results showed that the pretreatment of red sea bream with soak solutions could improve the viscoelasticity of fillets protein, stabilize the secondary and tertiary conformation of the MFP, inhibit the protein aggregation and oxidation, and decrease the degree of protein denaturation compared with the control (4 °C thawing), especially the soak solutions containing hAFP could minimize the freeze-thaw damage. To summarize, the hAFP helped to retain the above characteristics of frozen fillets much better than that of conventional cryoprotectants (glycerin) to improve the quality of the frozen product after thawing.

Keywords Herring antifreeze protein · Carboxymethyl chitosan magnetic nanoparticles · *Pagrosomus major* · Freeze-thaw damage · Protein oxidation

✉ Luyun Cai
lycai515@163.com

✉ Linyu Nian
15542846602@163.com

[1] Ningbo Research Institute, Zhejiang University, Ningbo 315100, China

[2] College of Biosystems Engineering and Food Science, National & Local Joint Engineering Laboratory of Intelligent Food Technology and Equipment, Zhejiang University, Hangzhou 310058, China

[3] Department of Food Quality and Safety/National R&D Center for Chinese Herbal Medicine Processing, College of Engineering, China Pharmaceutical University, Nanjing 211198, China

[4] National & Local Joint Engineering Research Center of Storage, Processing and Safety Control Technology for Fresh Agricultural and Aquatic Products, College of Food Science and Engineering, Bohai University, Jinzhou 121013, China

[5] Hangzhou Customs District, Hangzhou 310007, China

[6] College of Food Science, Southwest University, Chongqing 400715, China

Introduction

Antifreeze proteins (AFPs) are found in many organisms, such as fish, bacteria, insects, and plants. They are a family of proteins with thermal hysteresis activity (THA) that can lower the freezing point of the ice crystal without affecting melting temperature (Bar, Braslavsky, & Davies, 2016). They have the ability to inhibit ice crystal growth, hinder recrystallization caused by freeze-thaw cycles, and modify ice crystal morphology, which helps to enhance cellular integrity, reduce the degree of protein oxidation and degeneration, minimize tissue damage, and improve the products quality after freezing (Davies, 2014; Cruz, Vieira, & Silva, 2009). AFPs have been shown to be useful in living cells, tissue, and organs during chilled and frozen storage (Boonsupthip & Lee, 2010). All characteristics mentioned above make AFPs as promising additives used in food, cosmetic, and healthcare fields, especially as a natural ice modulator in the storage of frozen products, such as ice cream, frozen dough, meat, fish, fruits and

Published online: 23 December 2019

vegetables, and so on (Ohta & Yamada, 2011; Yeh, Kao & Peng, 2009; Ding et al., 2015; Kong et al., 2016, 2017).

Frozen storage is required to further prolong the shelf life and lower the deterioration rate of the finished food products. However, freezing can induce denaturation of the muscle proteins as the ice crystals grow in frozen foods caused by temperature fluctuation within the food during freezing and thawing cycles (Boonsupthip & Lee, 2010). Ice recrystallization causes the mechanical damage to tissues and cell structures including cell wall collapse, the reduction of water-holding capacity in food samples, and the increase of drip loss during thawing, ultimately resulting in a low-quality product (Kong, Hamid, Liu, & Sarojini, 2016). This denaturation can be prevented to some extent by cryoprotectants. For example, trehalose has the effect of reducing the freezing point of frozen products, and glycerin is a traditional cryoprotectant for cells freezing. AFPs application in frozen foods may inhibit recrystallization during freezing, storage, transport, and thawing, while AFPs solution had poor dispersion. Carboxymethyl chitosan magnetic nanoparticles (CCMN) were used to combine with herring antifreeze protein (hAFP) to improve the stability and uniformity of the solution.

Magnetic nanoparticles (MNPs) were mixed into cryogenic liquid to preserve the organ. The activity and function of the sample can be fully recovered after thawing (Manuchehrabadi et al., 2017). Cao et al. (2018) evaluated the effects of MNPs plus microwave or far-infrared thawing on protein conformation changes and moisture migration of red sea bream. Results showed that MNPs could help frozen fillets sustain a favorable quality. However, due to the oxidation, aggregation, and poor stability, the application of MNPs in the food industry was limited. CCMN are functional modification of MNPs, which chemical stability, biocompatibility, dispersibility, and water solubility were improved (Faraji, Yamini, & Rezaee, 2010). The -COOH on the carboxymethyl chitosan can form a stronger chemical bond with the -OH on the surface of MNPs, leading to a better adsorption layer on the surface of Fe_3O_4. Results showed that CCMN have a larger specific surface area to facilitate immobilization of the protein, improve the protein thermal stability and conformational stability (Liang & Zhang, 2007). On the other hand, AFPs showed the poor dispersion in the solution, while CCMN combined with AFPs could improve the stability, uniformity, and dispersion of the system. In this experiment, based on the successful application of AFPs in frozen food and the convenience and effectiveness of MNPs in practice, the CCMN combined with hAFP to pretreat the frozen fish on quality changes was investigated.

To our knowledge, the effects of CCMN plus hAFP on quality attributes in frozen seafood are unknown. The objective of this study was to examine how the hAFP and CCMN pretreatment affect the dynamic rheological property, protein structure, and aggregation and oxidation of red sea bream and evaluate their potential to minimize freeze-thaw damage in frozen products.

Materials and methods

Materials

Herring (*Clupea harengus*) and red sea bream (*Pagrosomus major*) were obtained from Qingdao Shunhaifu Commercial Trading Co., Ltd. (Qingdao, China). The fishes were added with ice to keep at 4 °C during transportation and were shipped to the laboratory within 12 h. Upon arrival, the fishes were quickly headed, gutted and peeled. These processing operations were controlled at 4 °C by ice addition to maintain the constant temperature. Trehalose was purchased from Henan Sanhua Biological Technology Co., Ltd. (Zhengzhou, China). Carboxymethyl chitosan magnetic nanoparticles (CCMN) were provided by Xian Ruixi Biological Technology Co., Ltd. (Xian, China). Bovine serum albumin and SDS-PAGE gel kit were purchased from Solarbio Science & Technology Co., Ltd. (Beijing, China). Ca^{2+}-ATPase and carbonyl content assay kit were purchased from Nanjing Jiancheng Bioengineering Institute (Nanjing, China). All other chemicals were of analytical grade. All experiments were performed at least in triplicate.

Sample Preparation

The extraction of antifreeze protein (AFP) was carried out according to the method of Evans and Fletcher (2010), and the extracted hAFP was identified as Ca^{2+} dependent type II AFP. The red sea bream meat was cut into small pieces (2 × 2 × 2 cm^3) and divided into four groups: NTC (the samples were soaked in 0.9% (w/v) NaCl solution containing 0.1 M trehalose and 0.01% (v/v) CCMN); NTC-G (the samples were soaked in 0.9% (w/v) NaCl solution containing 0.1 M trehalose, 0.01% (v/v) CCMN and 0.5 M glycerin); and NTC-hAFP0.1% (the samples were soaked in 0.9% (w/v) NaCl solution containing 0.1 M trehalose, 0.01% (v/v) CCMN and 0.1% (w/v) herring antifreeze protein). Non-treated red sea bream samples were used as control. Then four groups of samples were placed at 4 °C for 4 h and frozen in a − 20 °C refrigerator for 24 h. The frozen samples were thawed at 4 °C overnight.

Extraction of Red Sea Bream Myofibrillar Protein

The myofibrillar protein (MFP) extraction was done according to Xia, Kong, and Liu and Liu (2009) with slight modifications. The four groups of fillets were chopped to mince to

extract the MFP. The samples were dissolved in 4 volumes of 20 mM phosphate buffer solution (PBS, pH 7.0), homogenized at 3000 rpm for 3 min using a homogenizer (FJ300-SH, Shanghai Specimen and Model Factory, Shanghai, China) and centrifuged (Sorvall Stratos Centrifuge, Thermo Fisher Scientific, Waltham, MA, USA) at 5000 × g for 15 min at 4 °C. The sediment was dissolved in PBS (20 mM, pH 7.0) again. The above steps were repeated three times. After that, the sediment was dissolved in 4 volumes of PBS (20 mM, containing 0.6 M NaCl, pH 6.7) to be homogenized and centrifuged again. The supernatant was obtained, stored at 4 °C, and used in 24 h. The MFP solutions were diluted with PBS (20 mM, containing 0.6 M NaCl, pH 6.7). The protein concentration was determined by the Biuret method (Gornall, Bardawill, & David, 1949) using bovine serum albumin as a standard.

Determination of Dynamic Rheological Properties

The controlled stress rheometer (Discovery HR-1, TA Instrument Ltd, New Castle, DE, USA) with a 40 mm diameter parallel plate was used to determine the dynamic rheological characteristics by the method of Campo-Deaño et al. (2009) and Koch, Emin, and Schuchmann (2017). The MFP samples (30 mg/mL) were used to test the temperature, time, frequency, and stress sweeps. The storage modulus (G′) was recorded and expressed as Pa.

Temperature Sweep

The MFP samples were heated from 20 to 90 °C with a rate of 2 °C/min and tested at the strain amplitude, angular frequency, and truncation gap of 0.1%, 1.0 rad/s, and 500 μm, respectively (Mehta, & Nayak, 2017; Cao et al., 2018; Cai et al. 2018).

Time Sweep

The temperature, strain amplitude, angular frequency, and truncation gap of tested MFP samples were set at 4 °C, 0.1%, 1.0 rad/s, and 500 μm, respectively. The duration time was 30 min. The sampling interval was 10 s/pt.

Frequency Sweep

The temperature, strain amplitude, and truncation gap of tested MFP samples were set at 4 °C, 0.1%, and 500 μm, respectively. The angular frequency was ranged from 0.1–100 rad/s.

Amplitude Sweep

The temperature, angular frequency, and truncation gap of tested MFP samples were set at 4 °C, 1.0 rad/s, and 500 μm, respectively. The strain amplitude was ranged from 0.01–100%.

Determination of MFP Conformation

Raman Spectra

Raman spectra were measured according to the method of Xiong et al. (2016). About 0.5 mL MFP solutions (30 mg/mL) were put on a glass slide under the microscope and measured using a high-resolution Raman spectrometer (LabRAM HR Evolution, Horiba Jobin Yvon S.A.S, Paris, France). The instrument power was about 100 mW, and the frequency was calibrated by the monocrystalline silicon. The experiment was done at a slit width of 200 μm, a raster of 600 g/mm, a resolution ratio of 2 cm^{-1}, an access rate of 120 cm^{-1}•min^{-1}, and an integral time of 60 s. Raman spectra at 400–3600 cm^{-1} were conducted with deconvolution, second order derivative, and iterative curve fitting by PeakFit 4.12.

Intrinsic Fluorescence Spectra

Intrinsic fluorescence spectra were measured following the method by Cao and Xiong (2015) using a fluorescence spectrophotometer (970 CRT, Shanghai Precision and Scientific Instrument Co., Ltd, Shanghai, China). The MFP solutions were diluted to 0.1 mg/mL. The excitation wavelength was 280 nm, and the emission wavelength was from 300 to 400 nm. Both excitation and emission slits width were 10 nm, and the sensitivity was three.

Determination of MFP Aggregation

Surface Hydrophobicity (So-ANS)

The surface hydrophobicity of MFP was determined according to Lu, Zhang, Li, and Luo (2017) by ANS (8-anilino-1-naphthalene sulfonate) as a probe using a fluorescence spectrophotometer. The MFP was suspended in 20 mM PBS (containing 0.6 M NaCl, pH 6.7), and the protein concentration was adjusted to 0.2, 0.3, 0.5, and 1.0 mg/mL. Then 2 mL protein solutions were added to 10 μL 0.1 M potassium phosphate buffer (containing 8 mM ANS, pH 7.0) and mixed well. So-ANS of each sample was calculated from the slope of the relative fluorescence to protein concentration. The excitation wavelength was 390 nm, the emission wavelength was 470 nm, and both excitation and emission slits width were 5 nm.

Particle Size

Particle size was determined as described by Cosminm and Carmeni (2011) using a Brookhaven 90Plus nanoparticle size analyzer equipped with a Peltier temperature control system

(Brookhaven Instruments Corp., Holtsville, NY, USA). About 3 mL MFP solutions (2 mg/mL) were passed through 0.22 μm cellulose acetate membrane (water system), and the particle size of samples was measured at 25 °C, a fixed 90° angle, and 658 nm wavelength.

Zeta Potential

Zeta potential was measured using a Brookhaven 90Plus nanoparticle size analyzer (Brookhaven Instruments Corp., Holtsville, NY, USA). The pretreatment of sample was the same as that of particle size. The parameters were as follows: a 35 mW solid-state laser, λ = 660 nm, in the "High Precision" mode at 25 °C, and setting "water" as solvent (Cosminm & Carmeni, 2011).

Determination of MFP Oxidation

Solubility

The MFP solutions were diluted to 3 mg/mL and placed at 4 °C for 1 h then centrifuged at 5000 × g for 15 min at 4 °C to get the supernatant. Protein solubility was calculated using the following equation (Ko et al., 2016):

$$\text{Solubility}(\%) = \frac{\text{Protien concentration in the supernatant}}{\text{Protien concentration in solution}(3\ \text{mg/mL})} \times 100\%$$

Total Sulfhydryl (T-SH) and Disulfide Bond (SS) Contents of MFP

Determination of T-SH/ SS content was performed according to the method of Lv et al. (2018) and Lu et al. (2017) with slight modifications. A 1 mL MFP solution (4 mg/mL) was mixed with 9 mL 0.2 M Tris-HCl buffer (pH 8.0, containing 8 M urea, 1% SDS, and 3 mM EDTA)/0.2 M Tris-HCl buffer (pH 8.0, containing 8 M urea, 1% SDS, 3 mM EDTA, and 0.1 M Na_2SO_3) and mixed uniformly. Then the mixture (4 mL) was added to 0.2 M Tris-HCl buffer (pH 8.0, containing 10 mM DTNB)/0.2 M Tris-HCl buffer (pH 9.5, containing 8 M urea, 1% SDS, 3 mM EDTA, 0.1 M Na_2SO_3, and 1% NTSB (v/v)) and incubated at 40 °C for 25 min. The absorbance was measured at 412 nm using a solution of 0.6 M NaCl (pH 7.0) as the blank. T-SH/SS was calculated using the following equations:

$$\text{T-SH/SS}\left(\text{mol}/10^5\text{g pro}\right) = \frac{(\text{A}-\text{A}_0)*\text{d}}{(\text{c}*\varepsilon)}$$

where A refers to the absorbance of the experimental sample, A_0 refers to the absorbance of the blank sample, c = protein concentration (4 mg/mL), ε = extinction coefficient (13600·M^{-1}·cm^{-1}), and d = dilution factor (11.25).

Carbonyl Content of MFP

The MFP carbonyl content was determined according to the instructions of the carbonyl content kit (A087) by the method of Lu et al. (2017) with slight modifications. About 0.1 mL MFP (2 mg/mL) solution was added to 0.4 mL 10 mM 2, 4-Dinitrophenylhydrazine (DNPH, the solvent was 2 M HCl) and reacted at room temperature for 1 h in the darkroom. Then the mixture was added to 1 mL, 20% trichloroacetic acid (TCA, w/v) and centrifuged at a speed of 10,000 g for 10 min to get the sediment. The sediment was washed three times with 1 mL of ethanol/ethylacetate (1:1, v/v) to remove the unreacted reagents. After that, the precipitate was dissolved in 1.25 mL of 6 M guanidine in 2 M HCl and placed in water bath (37 °C) for 15 min to dissolve the precipitate and then centrifuged at a speed of 10,000 g for 5 min to get the supernatant. The absorbance was measured at 370 nm, and the solution of 2 M HCl was replaced by DNPH as the control. The carbonyl content was expressed as nmol/mg of protein, which was calculated using the following equation:

$$\text{Carbonyl content}(\text{nmol/mg pro}) = \frac{\text{A}-\text{A}_0}{\varepsilon\ \text{b}\ \text{c}} \times 12.5 \times 10^6$$

where A refers to the absorbance of the experimental sample, A_0 refers to the absorbance of the control sample, ε = absorption coefficient (22·mM^{-1}·cm^{-1}), 12.5 = $V_{guanidine}/V_{MFP}$ = 1.25 mL/0.1 mL, b = light diameter of a quartz dish (1 cm), and c = protein concentration (2 mg/mL).

Dityrosine Content of MFP

Dityrosine content was measured using a fluorescence spectrophotometer (970 CRT, Shanghai Precision and Scientific Instrument Co., Ltd, Shanghai, China) according to the method of Davies, Delsignore, and Lin (1987) with slight modifications. MFP solutions (1 mg/mL) were centrifuged at 5000 g for 5 min to remove the insoluble substance. The excitation and emission wavelength was 325 nm and 420 nm, respectively, both slit width were 10 nm, and the sensitivity was 2. The dityrosine content was expressed by the measured fluorescence value (AU).

Ca^{2+}-ATPase Activity of MFP

Ca^{2+}-ATPase activity was detected by quantifying phosphorus according to the instructions of the ATPase kit (A070-3) by the method of Mao et al. (2016). ADP and inorganic phosphate (Pi) were generated from hydrolysis of ATP by ATPase, which can be measured in a simple colorimetric reaction.

Ca^{2+}-ATPase activity was expressed as the amount of inorganic phosphate produced per minute per milligram of tissue protein (μmol (Pi)/mg (pro)/min).

Sodium Dodecyl Sulfate-Polyacrylamide Gel Electrophoresis (SDS-PAGE)

SDS-PAGE was performed by Cao et al. (2018). MFP samples (4 mg/mL) were boiled for 5 min. Then 10 μL protein marker (0.9 μg/μL, Takara, Dalian Bioengineering Co. Ltd, Dalian, China) and 10 μL MFP solutions were loaded into the polyacrylamide gel with 12% running gel and 5% stacking gel. Electrophoresis was performed at 80 V for the stacking gel and 120 V for the resolving gel. The gels were stained with Coomassie brilliant blue R-250, and destained with aqueous solution containing 25% absolute ethyl alcohol and 8% glacial acetic acid until the solution was clear. The gels were scanned, and the images were captured and analyzed using a calibrated densitometer (GS800, Bio-Rad Laboratories, Inc., CA, USA).

Data Analysis

One-way analyses of variance (ANOVA) were used to analyze data following a Duncan's multiple range test, expressed as mean ± standard deviation (SPSS 22.0, Chicago, IL, USA). $P < 0.05$ was considered as significant. Raman spectra were analyzed by PeakFit 4.12 (SPSS Inc., Chicago, IL, USA). All figures were obtained by Origin Pro 8.5 (OriginLab Co., Northampton, MA, USA).

Results and Discussion

Dynamic Rheology

The dynamic rheology was performed to evaluate the viscoelasticity of protein. The storage modulus (G′) represented the energy stored per cycle of sinusoidal shear deformation, which mainly indicated the denaturation, unfolding and aggregation of protein, and the formation of three-dimensional gel network structure of protein. (Peng, Li, Ding, & Yang, 2017). Campo-Deaño et al. (2009) elucidated the effect of rheological properties on giant squid surimi when added different cryoprotectants; results indicated that trehalose favored less initial protein aggregation and hence a thermorheologically stable structure. Yeh, Kao, and Peng (2007) elaborated that the addition of AsAFPs in frozen dough can reduce the damage of ice crystals to the frozen dough system by inhibiting the recrystallization of ice crystals and increase the viscoelasticity during the freezing process. The effect of soak solutions on G′ values of MFP extracted from red sea bream were determined as a function of temperature, time, frequency, and amplitude (Fig. 1A, 1B, 1C, 1D).

Temperature Sweep

The change curve of G′ of MFP in the heating process reflected the process of protein denaturation, aggregation, and spatial network formation. As shown in Fig. 1A, the G′ of MFP extracted from the NTC-$hAFP_{0.1\%}$ sample was the highest, which was higher than those extracted from NTC and NTC-G samples, presumably due to more extensive secondary molecular interactions and disulfide cross-links. (Sun & Arntfield, 2012). During the freezing and thawing, the ice crystals destroyed the cell structure, protein was oxidized and denatured, and the ability to form three-dimensional network was weakened. Results indicated that trehalose, glycerin, and hAFP all have the function on cryoprotection. AFPs can inhibit the growth of ice crystals and prevent protein denaturation, CCMN plus hAFP had the effect on freezing protection of red sea bream myofibril, and 0.1% hAFP could be used as a substitute for glycerin applied in the field of thawing.

Time Sweep

From Fig. 1B, the G′ values of MFP extracted from red sea bream fillets were increased rapidly ranged from 0–200 s; after that, the growth was decreased and tended to stabilize. During time sweep, the initial increase in G' is attributable to time-dependent formation of molecular entanglements and network structure (Langevin, 2014). From Fig 1B, the G' of NTC-$hAFP_{0.1\%}$ was the highest, which was mainly due to the hAFP that had the effect of forming small ice crystals and reducing cell damage on frozen food (Ding et al., 2015). Therefore, it would be advantageous to pre-treat by trehalose and CS@Fe_3O_4 nanoparticle combine with hAFP or glycerin solutions, which could prevent protein degradation and maintain the protein network structure.

Frequency Sweep

Figure 1C showed that the G′ values were increased within the range of angular frequency (0.1–100 rad/s), indicating that the whole gel system had not been completely formed. The soak solutions pretreatment on red sea bream could increase the G′ values and improve the stability of myofibrillar protein system, and the gel performance of myofibril in three-dimensional gel network was enhanced. The G′ of NTC-$hAFP_{0.1\%}$ was the highest, which was in accordance with temperature and time sweeps.

Amplitude Sweep

Amplitude sweep was used to study the fracture mechanism of interfacial film. Figure 1D showed the G′ of the interface changes with strain, when the strain increased to about 2%, G′ of samples began to decrease sharply, indicating that the

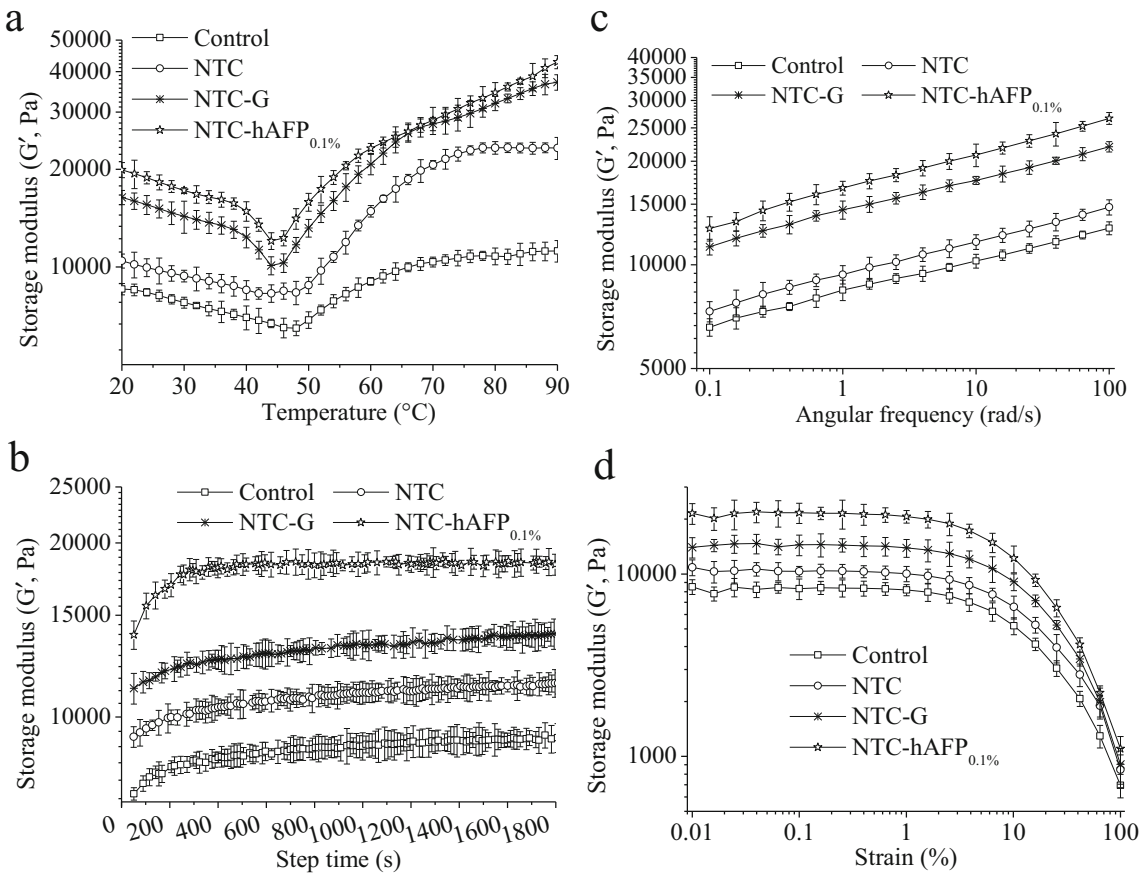

Fig. 1 Effect of soak solutions pretreatment on dynamic rheology with temperature (**A**), time (**B**), frequency (**C**), and amplitude (**D**) sweeps of red sea bream. Control (□), NTC (NaCl + Trehalose + CCMN) (○), NTC-G (NaCl + Trehalose + CCMN + Glycerin) ( ), NTC-hAFP$_{0.1\%}$ (NaCl + Trehalose + CCMN + 0.1% (w/v) herring antifreeze protein) (☆)

interfacial film structure began to be damaged. The G′ of NTC-hAFP$_{0.1\%}$ was the highest, which was consistent with the temperature, time, and frequency sweeps.

Analyses of MFP Conformation

Raman Spectrum

Raman spectrum was used to explain the structure changes in protein by the stretching vibration of C=O bond and the flexural vibration of C–N, C_α–C–N, and N–H bonds inside the polypeptide chain (Zhang et al., 2016). The Raman spectra were smoothed and baseline corrected as shown in Fig. 2A. Table 1 showed the tentative assignment of selected bands in the Raman spectra of proteins.

Choosing amide I region (1600~1700 cm^{-1}) to conduct with deconvolution, second order derivative and iterative curve fitting, and the content of protein secondary structure was calculated in Fig. 2B, including α-helix (1645~1658 cm^{-1}), β-sheet (1665~1680 cm^{-1}), random coil (1660~1665 cm^{-1}), and β-turn (1680 cm^{-1}). α-helix and β-sheet represent the conformation regularity of protein, while random coil and β-turn represent the conformation looseness of protein (M. Hernández-Martínez, et al., 2014). From Fig. 2B, the α-helix content of control, NTC, NTC-G, and NTC-hAFP$_{0.1\%}$ samples was 39.74%, 42.87%, 47.19%, and 56.91%, the β-sheet content was 29.41%, 28.41%, 26.6%, and 19.86%, and the random coil content was 23.15%, 21.76%, 18.82%, and 15.5%, respectively. In the pretreatment of fillets by soak solutions before freezing, the α-helix content was increased while the β-sheet and random coil contents were decreased, which indicated that the structure of protein was transformed from loose to regular. The cause of this phenomenon is mainly because CS@Fe_3O_4 nanoparticle combined with hAFP or glycerin can reduce ice crystal size and help to minimize the freeze damage on cell structure (Kong et al., 2017). There was no significant difference in β-turn of treatment groups compared to the control. After freezing and thawing, the protein denaturation and sulfhydryl oxidation led to the destruction of secondary structure of protein. Result showed that the protein structure of NTC-hAFP$_{0.1\%}$ was the most stable.

Amide III region (1230–1350 cm^{-1}) is a conformation sensitive band of Raman spectrum, which provides the vibration information of the polypeptide chain conformation. From Fig.

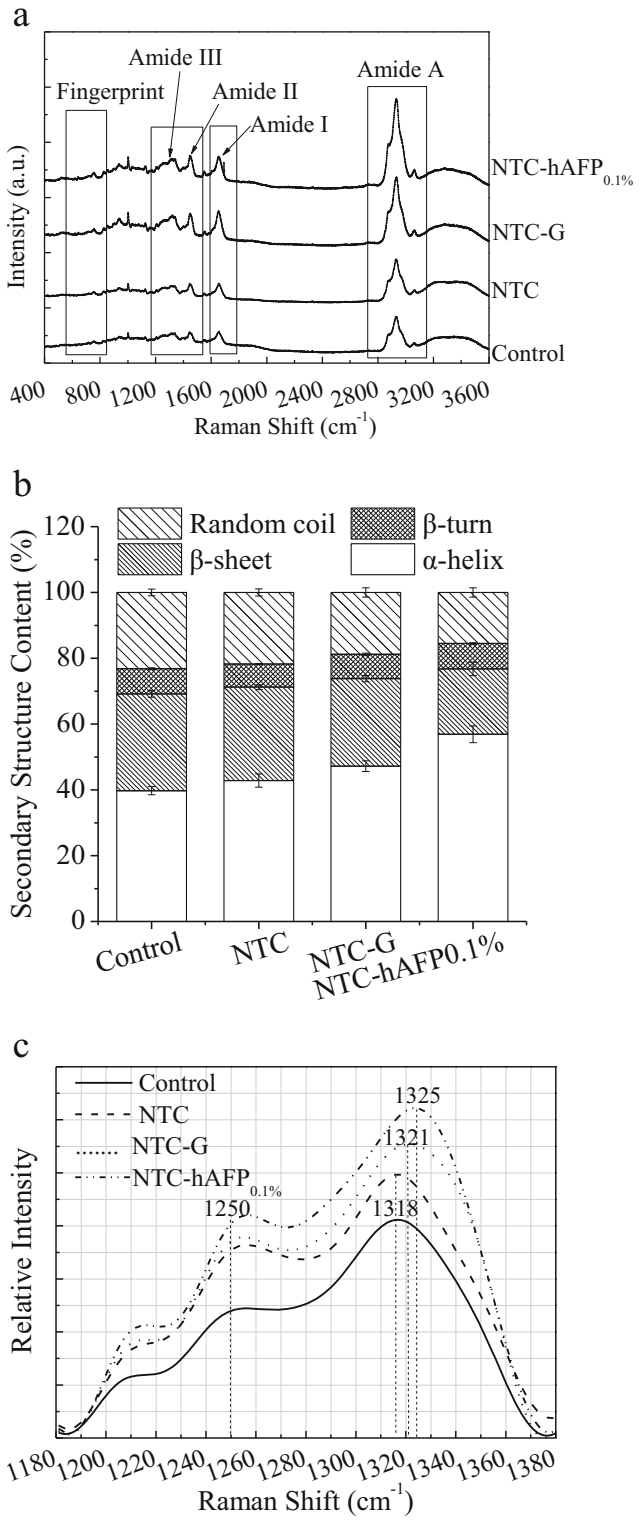

Fig. 2 Effect of soak solutions pretreatment on Raman spectra (**A**), secondary structure content (**B**) and amide III region of Raman spectra (**C**) of red sea bream. (Control (—), NTC (NaCl + Trehalose + CCMN) (- - -), NTC-G (NaCl + Trehalose + CCMN + Glycerin) (·····), NTC-hAFP$_{0.1\%}$ (NaCl + Trehalose + CCMN + 0.1% (w/v) herring antifreeze protein) (–▪–)

2C, the Raman peaks of red sea bream protein were shown in 1318 cm^{-1}, 1318 cm^{-1}, 1321 cm^{-1}, and 1325 cm^{-1}, respectively. Compared to the control, the treatment groups shifted toward to the large wave number, and the relative peak strength was increased, which indicated that the α-helix content was increased in fish protein. Carew, Asher, and Stanley (1975) found that the bands near 1250 cm^{-1} and 1315 cm^{-1} are formed respectively by the α-helix structure in the head and tail regions of myosin globular and fibrous structures.

The characteristic vibration band of disulfide bond was around 500–550 cm^{-1}. The conformation "gauche-gauche-trans" and "trans-gauche-trans" appeared at near 525 cm^{-1} and 545 cm^{-1}, respectively (Herrero, 2008). As shown in Fig. 3A, the Raman peaks of the control, NTC, NTC-G, and NTC-hAFP$_{0.1\%}$ samples appeared respectively at 525 cm^{-1}, 528 cm^{-1}, 532 cm^{-1}, and 556 cm^{-1}, which indicated that the peak had a red shift (to longer wavelengths). The disulfide bond conformation of the control and NTC samples was "gauche-gauche-trans," while the NTC-G, NTC-hAFP$_{0.1\%}$ was "trans-gauche-trans," and the latter conformation is more stable. Therefore, the trehalose and CCMN combined with glycerin or hAFP applied to freezing and thawing of red sea bream could improve the stability of MFP.

The strong band was formed near 2900 cm^{-1} by C–H stretching vibration of aromatic amino acids, peptides, and proteins (Fig. 3B). The peak of 2933 cm^{-1} was caused by the symmetric stretching vibration of CH_3 or the CH_2 asymmetric expansion vibration, while the sub-peak of 2878 cm^{-1} was due to the asymmetric expansion of CH_2 (Sun et al., 2011). The relative intensity was of the order control < NTC < NTC-G < NTC-hAFP$_{0.1\%}$. The relative intensity was lower in the control arising from the diminished exposure of aromatic amino acids due to hydrophobic aggregation (Zhang et al., 2016). The effect of 0.1% hAFP on protecting fish protein structure was similar to the traditional cryoprotectant (glycerin).

Intrinsic Fluorescence Spectrum

The intrinsic fluorescence spectrum reflects the degree of protein oxidation and the changes of microenvironment of tryptophan residues. As shown in Fig. 3C, there was no significant difference between control and NTC samples on maximum position of fluorescence peak (λ_{max}) and fluorescent intensity (FI) ($P > 0.05$). There were two reasons for the low FI values in the control samples. The one was the formation of ice crystals in freezing process that destroyed the integrity of the tissue and caused the degree of protein oxidation increased. This led to protein aggregation, tryptophan residues embedding. The other was the tryptophan in the protein side chain which was oxidized and quenched, which brought about protein cross-linking and aggregation (Liu et al., 2015; Cao et al., 2018). λ_{max} of NTC-G and NTC-hAFP$_{0.1\%}$ had a red shift (to longer

Table 1 Assignment of Raman modes useful in the interpretation of protein structure

Raman shift (cm^{-1})	Assignment and remarks
500–550	S–S stretching vibration
757–1340	Tryptophan stretching vibration
830–850	Fermi bimodal, tyrosine residues microenvironment
940	C–C stretching vibration
1004 ± 2	Phenylalanine ring stretching vibration
1230–1350	Amide III region: N–H bend stretch coupled C–N stretch
1500–1600	Amide II region: bending vibrations of N–H groups and stretching vibrations of C–N groups
	CH_2 bending (scissors) vibration
1600–1700	Amide I region: C=O stretching/hydrogen bonding coupled with COO^-
2900	C–H antisymmetric and symmetric stretching

wavelengths), and NTC-hAFP$_{0.1\%}$ sample had the highest λ_{max} and FI values, which indicated that CCMN plus hAFP could improve the stability, uniformity, and dispersion of the system and reduce the degree of protein oxidation.

Analyses of MFP Aggregation

Surface Hydrophobicity (S_0-ANS)

The S_0-ANS of proteins reflects the relative content of hydrophobic amino acids on protein surface, which can be used to measure the degree of protein degeneration. After freezing and thawing, the amino acid side chain was oxidized, which changed the protein conformation, and the hydrophobic amino acid residues inside the protein may become exposed to the surface of the molecule, increasing the hydrophobicity of the protein (Shi et al., 2015). From Fig. 4A, results indicated that the pretreatment of red sea bream before frozen could decrease the S_0-ANS of myofibrillar protein. The NTC had no marked effects on So-ANS compared to control, and there was no significant difference between NTC-G and NTC-hAFP$_{0.1\%}$ ($P > 0.05$). With the pretreatment of soak solutions, the β-sheet of the thawed fish protein turned into α-helix gradually (Fig. 2B), and the protein structure was more stable; the effects of inhibiting protein oxidation and preventing the exposure of the hydrophobic groups of aliphatic and aromatic amino acids were increased. Therefore, results showed that CCMN plus glycerin or hAFP could modify the morphology of ice crystals, protect cell membranes, and decrease the degree of protein oxidation.

Particle Size

The result of the particle size measurement was shown in Fig. 4A. The average effective particle diameter (d_{eff}) was 1470.85 ± 23.96, 1354.45 ± 16.77, 1159.59 ± 3.07, and 1090.25 ± 17.99 nm corresponding to control, NTC, NTC-G, and NTC-hAFP$_{0.1\%}$. The bigger d_{eff} of protein indicated that the MFP tended to aggregate, which caused the exposure of hydrophobic groups and decreased the degree of hydrophobic group coils on the protein and the poorer stability of system, and the So-ANS was increased. Results proved that hAFP had the effect of inhibiting the growth of the crystals, reducing cell damage and protein oxidation on frozen food. Therefore, CCMN plus glycerin or hAFP could inhibit the aggregation of MFP and decrease the d_{eff} and S_0-ANS of protein.

Zeta Potential

The side chains of protein molecules contain many polar groups (such as carboxyl, hydroxyl, and amine) and nonpolar groups. The hydrophilic of polar groups are exposed to the surface of the protein in aqueous solution, causing the surface to be charged. Zeta potential (ζ) was used to measure the electrical charge of proteins and as a relative indicator for the colloidal stability of the protein systems (Beliciu & Moraru, 2011). When the ζ absolute value (|ζ|) of the protein solution was smaller, the same charges of protein surface were less, which could decrease the electrostatic repulsion and make the system of protein molecules tend to aggregate, so the stability of solution was reduced. This phenomenon would cause hydrophobic groups that inside of the protein exposed, and the S_0-ANS was increased (Wong, Li, & Augustin, 2011); otherwise it was decreased.

As shown in Fig 4A, the ζ of control was − 26.33 ± 2.03 mV, which meant the threshold of delicate dispersion of protein solution. The ζ of NTC and NTC-G was − 31.24 ± 1.35 and − 38.02 ± 1.62 mV, respectively, and − 30 to − 40 mV indicated the moderate stability of solution (Beliciu & Moraru, 2011). NTC-hAFP$_{0.1\%}$ ζ value was − 45.26 ±

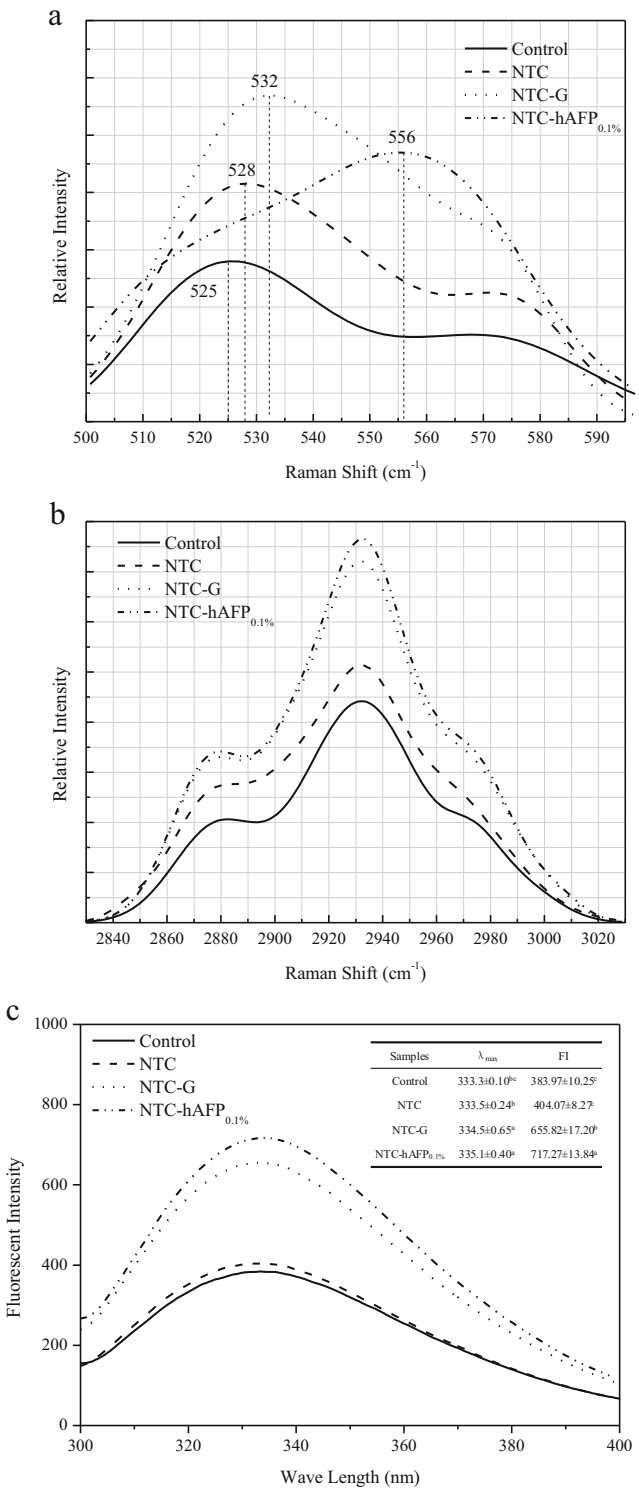

Fig. 3 Effect of soak solutions pretreatment on disulfide bond of Raman spectra (**A**), C–H stretching vibrations of Raman spectra (**B**), and intrinsic fluorescence spectra (**C**) of red sea bream

1.05 mV, implying the good stability of solution. This is possibly a direct result of CCMN plus hAFP that could retard the protein oxidation and improve the system stability.

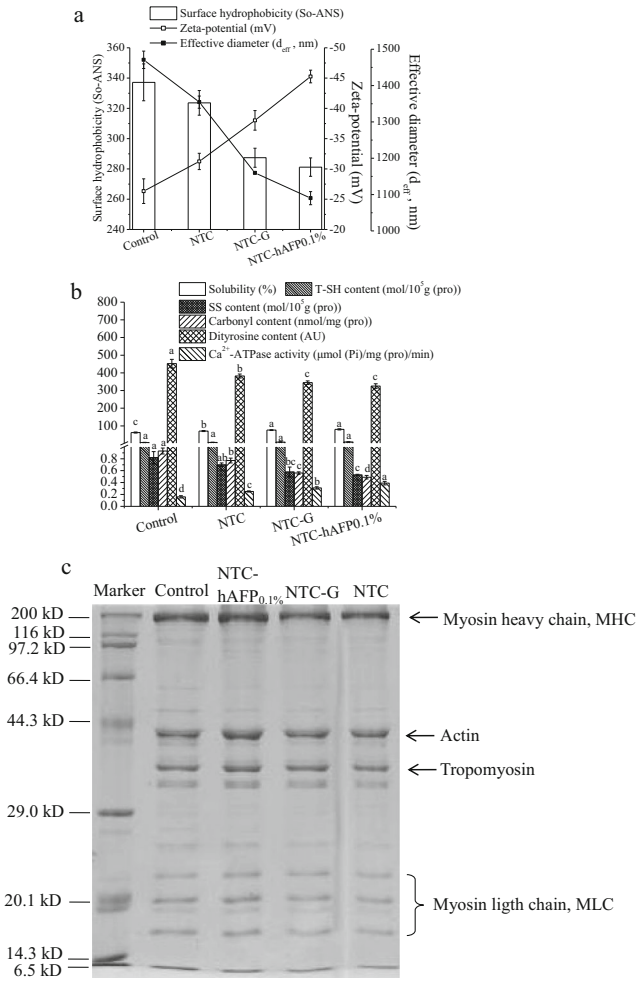

Fig. 4 Effect of soak solutions pretreatment on So-ANS, particle size, and zeta-potential (**A**), protein oxidation index (solubility, total sulfhydryl, disulfide bond, carbonyl, dityrosine, Ca^{2+}-ATPase activity) (**B**), and SDS-PAGE (**C**) of red sea bream

Analyses of MFP Oxidation

Solubility

The solubility of protein reflects the degree of protein degradation, and the decrease of solubility is a sign of protein degeneration (Ko et al., 2016). As shown in Fig. 4B, the control samples had the lowest solubility, possibly due to the oxidation, cross-linking, and aggregation of proteins during

freezing and thawing. Compared to the control, the MFP solubility was increased by 8.63%, 13.94%, and 17.92%, corresponding to NTC, NTC-G, and NTC-hAFP$_{0.1\%}$, respectively. This was because CCMN plus glycerin/hAFP could inhibit the mechanical damage and protein degeneration of muscle cell membranes and organelles caused by ice crystals, and 0.1% hAFP could be used as the substitute for the traditional antifreeze (glycerin) applied to freezing and thawing fields.

Total Sulfhydryl (T-SH) and Disulfide Bond (SS)

Many studies showed that changes in the structure of actin head region would expose the sulfhydryl that was buried inside the protein, which led to the oxidation of sulfhydryl transform into disulfide bond, resulting in a decrease in the content of sulfhydryl and an increase in the content of disulfide bond. Therefore, the content of sulfhydryl and disulfide bond can be used as important indicators of protein oxidation (Zhang et al., 2015; Lv et al., 2018). The changes in T-SH and SS contents based on the protein denaturation were shown in Fig. 4B. The content of T-SH was 5.95 ± 0.14, 6.75 ± 0.34, 8.48 ± 0.62, and 8.82 ± 0.48 mol/10^5 g pro, and the SS content was 0.82 ± 0.1, 0.7 ± 0.03, 0.58 ± 0.08, and 0.53 ± 0.01 mol/10^5 g pro, corresponding to control, NTC, NTC-G, and NTC-hAFP$_{0.1\%}$, respectively. During freezing and thawing, the sulfhydryl groups were exposed and oxidized to SS, resulting in the lowest content of T-SH and the highest content of SS in control samples. The CCMN combined with glycerin/hAFP have the effect on preventing the oxidation of sulfhydryl groups and disulfide interchange. There was no significant difference ($P \geq 0.05$) between NTC-G and NTC-hAFP$_{0.1\%}$ in the content of T-SH and SS.

Carbonyl Content

In the oxidation process, the amino (NH- or NH_2-) on the side chain of the protein is very sensitive to hydroxyl (OH-), these free radicals may undergo nucleophilic attack on the protein methylene carbon and can extract a hydrogen atom, triggering a free radical chain reaction and forming carbonyl groups (Gonçalves, 2009). Protein carbonylation is the most commonly used biomarker for protein oxidation, and carbonyl content reflects the degree of protein oxidation (Zhang et al., 2015). As shown in Fig. 4B, the carbonyl content of control, NTC, NTC-G, and NTC-hAFP$_{0.1\%}$ was 0.93 ± 0.05, 0.77 ± 0.04, 0.56 ± 0.02, and 0.49 ± 0.03 nmol/mg pro, respectively. This phenomenon can be attributed to the formation of ice crystals during freezing that causes cell rupture, leading to the release of proteases such as cathepsins, matrix metalloproteinase (MMP), and oxidases such as cytochrome oxidase and lipoxygenase (Nielsen & Jørgensen, 2004) and pro-oxidants including reactive oxygen species (ROS) (Xia, Kong, Liu & Liu, 2009), speeding up the oxidation of fat and protein. Results indicated that NTC-G and NTC-hAFP$_{0.1\%}$ samples could reduce the ice crystals size, modify their morphology, and prevent the oxidation of protein, resulting in a decrease in the content of carbonyl.

Dityrosine Content

During the oxidation process, tyrosine is attacked by free radicals and forms covalent cross-links with the active amino acid residues of other proteins, including complexation between two tyrosine residues to form dityrosine. Therefore, the content of dityrosine is one of the specific biomarkers for protein oxidation (Colombo et al., 2015). As shown in Fig. 4B, the dityrosine content of control, NTC, NTC-G, and NTC-hAFP$_{0.1\%}$ was 452.47 ± 24.26, 382.36 ± 11.38, 344.65 ± 10.03, and 25.32 ± 13.12 AU, respectively. There was no significant difference between NTC-G and NTC-hAFP$_{0.1\%}$ ($P \geq 0.05$). The results proved that CS@Fe_3O_4 nanoparticle plus hAFP can inhibit the oxidation and degeneration of protein, and hAFP could replace the glycerin used in the field of freezing and thawing.

Ca^{2+}-ATPase Activity

The myosin head region has the action site of Ca^{2+}-ATPase, so the Ca^{2+}-ATPase activity can reflect the denaturation of myosin head (Lv et al., 2018). The decrease of Ca^{2+}-ATPase activity was due to the oxidation of sulfhydryl in the myosin head and the cross-linking of protein. Therefore, the Ca^{2+}-ATPase activity is often considered to indicate freezing or thermal denaturation of myosin (Jantakoson, Thavaroj, & Konno, 2013). Figure 4B showed the Ca^{2+}-ATPase activity of different samples was 0.16 ± 0.02, 0.25 ± 0.01, 0.31 ± 0.02, and 0.39 ± 0.03 μmol (Pi)/mg (pro)/min, corresponding to control, NTC, NTC-G, and NTC-hAFP$_{0.1\%}$, respectively. The result demonstrated that the Ca^{2+}-ATPase activity was increased significantly ($P < 0.05$), which showed that the head structure of myosin was influenced slightly by the hAFP$_{0.1\%}$, indicating that the hAFP as a cryoprotectant could alleviate protein oxidation and maintain the integrity of the myosin head structure and high content of Ca^{2+}-ATPase activity.

Analyses of SDS-PAGE

The SDS-PAGE of samples was shown in Fig. 4C. Electrophoretic analysis of the salt-soluble fraction indicated the existence of several myofibrillar proteins, including myosin heavy chain (MHC, about 200 kDa), actin (45 kDa), tropomyosin (38 kDa), and myosin light chain (MLC, 20–30 kDa); the results were similar to Gómez-Estaca, Montero, and Gómez-Guillén (2014). The appearance of MHC may be caused by the cross-linking and aggregation of myofibril protein. As shown in Fig. 4C, the MHC bands were partially

dissociated, which may be due to the high activity of cathepsin in muscle fibers under cold storage, causing severe protein degradation and shallow MHC electrophoretic bands, while MLC indicating that oxidation caused fragmentation of MHC. From Fig. 4C, all electrophoretic bands of control sample showed lower intensity than other samples, which was mainly due to a severe oxidation during freezing and thawing. The NTC and NTC-G samples exhibited a dramatic reduction in actin, tropomyosin, and MLC compared to NTC-hAFP$_{0.1\%}$, which was due to the oxidation causing a reduction in the band intensity. Therefore, CCMN plus hAFP had a significant effect on preventing protein degradation of thawed red sea bream fillets.

Conclusions

The effectiveness of hAFPs pretreatment has related to inhibiting the ice crystal growth, modifying ice crystal sharp and preventing the protein oxidation. The hAFPs pretreatment before frozen could help to increase the G' values. From Raman spectrum, the α-helix content was increased, which indicated the protein secondary structure was transformed from loose to regular. The intrinsic fluorescence spectrum, So-ANS, particle size, and zeta potential indicated that the hAFPs pretreatment could help to inhibit protein oxidation and aggregation, prevent the exposure of the hydrophobic groups, and improve the system stability. Results of solubility, T-SH, SS, carbonyl and dityrosine content, Ca^{2+}-ATPase activity, and SDS-PAGE showed hAFPs pretreatment could inhibit oxidation and denaturation of MFP, and hAFPs provided better protection than conventional cryoprotectants such as glycerin. In conclusion, the hAFPs could be used as a beneficial additive to froze food and help to address the cost issue to realize their potential in cryopreservation.

Funding Information This study was supported by the National Key R&D Program of China (2018YFD0901106), the Science and Technology Project by General Administration of Quality Supervision, Inspection and Quarantine of China (2017IK090), the National Natural Science Foundation of China (31401478), the Natural Science Foundation of Liaoning Province of China (20170540006), and the Aquatic Products Processing and Safety Key Laboratory of Guangdong Province (GDPKLAPPS1805).

Compliance with Ethical Standards

Conflict of Interest The authors declare that they have no conflict of interest.

References

Bar, D. M., Braslavsky, I., & Davies, P. L. (2016). Ice-binding proteins and their function. *Annual Review of Biochemistry, 85*, 515–542.

Beliciu, C. M., & Moraru, C. I. (2011). The effect of protein concentration and heat treatment temperature on micellar casein-soy protein mixtures. *Food Hydrocolloids, 25*(6), 1448–1460.

Boonsupthip, W., & Lee, T. C. (2010). Application of antifreeze protein for food preservation: effect of type III antifreeze protein for preservation of gel-forming of frozen and chilled actomyosin. *Journal of Food Science, 68*(5), 1804–1809.

Carew, E. B., Asher, I. M., & Stanley, H. E. (1975). Laser Raman spectroscopy–new probe of myosin substructure. *Science, 188*(4191), 933–936.

Campo-Deaño, L., Tovar, C. A., Pombo, M. J., Solas, M. T., & Borderías, A. J. (2009). Rheological study of giant squid surimi (*Dosidicus gigas*) made by two methods with different cryoprotectants added. *Journal of Food Engineering, 94*(1), 26–33.

Cao, M. J., Cao, A. L., Wang, J., Cai, L. Y., Regenstein, J., Ruan, Y. J., & Li, X. X. (2018). Effect of magnetic nanoparticles plus microwave or far-infrared thawing on protein conformation changes and moisture migration of red sea bream (*Pagrus major*) fillets. *Food Chemistry, 266*, 498–507.

Cao, Y., & Xiong, Y. L. (2015). Chlorogenic acid-mediated gel formation of oxidatively stressed MP. *Food Chemistry, 180*, 235–243.

Cai, L., Cao, M., Cao, A., Regenstein, J., Li, J., & Guan, R. (2018). Ultrasound or microwave vacuum thawing of red sea bream (*Pagrus major*) fillets. *Ultrasonics Sonochemistry, 47*, 122–132.

Colombo, G., Clerici, M., Giustarini, D., Portinaro, N., Badalamenti, S., Rossi, R., et al. (2015). A central role for intermolecular dityrosine cross-linking of fibrinogen in high molecular weight advanced oxidation protein product (aopp) formation. *Biochim Biophys Acta, 1850*(1), 1–12.

Cosminm, B., & Carmeni, M. (2011). The effect of protein concentration and heat treatment temperature on micellar casein-soy protein mixtures. *Food Hydrocolloids, 25*(6), 1448–1460.

Cruz, R. M. S., Vieira, M. C., & Silva, C. L. M. (2009). The response of watercress (*Nasturtium officinale*) to vacuum impregnation: Effect of an antifreeze protein type I. *Journal of Food Engineering, 95*(2), 339–345.

Davies, P. L. (2014). Ice-binding proteins: a remarkable diversity of structures for stopping and starting ice growth. *Trends in Biochemical Sciences, 39*(11), 548–555.

Davies, K. J. A., Delsignore, M. E., & Lin, S. W. (1987). Protein damage and degradation by oxygen radicals. ii. modification of amino acids. *Journal of Biological Chemistry, 262*(20), 9902–9907.

Ding, X., Zhang, H., Wang, L., Qian, H., Qi, X., & Xiao, J. (2015). Effect of barley antifreeze protein on thermal properties and water state of dough during freezing and freeze-thaw cycles. *Food Hydrocolloids, 47*, 32–40.

Evans, R. P., & Fletcher, G. L. (2010). Type I antifreeze proteins expressed in snailfish skin are identical to their plasma counterparts. *Febs Journal, 272*(20), 5327–5336.

Faraji, M., Yamini, Y., & Rezaee, M. (2010). Magnetic nanoparticles: synthesis, stabilization, functionalization, characterization, and applications. *Journal of the Iranian Chemical Society, 7*(1), 1–37.

Gómez-Estaca, J., Montero, P., & Gómez-Guillén, M. C. (2014). Shrimp (*Litopenaeus vannamei*) muscle proteins as source to develop edible films. *Food Hydrocolloids, 41*(41), 86–94.

Gonçalves, A. A. (2009). Ozone - an emerging technology for the seafood industry. *Brazilian Archives of Biology & Technology, 52*(6), 1527–1539.

Gornall, A. G., Bardawill, C. J., & David, M. M. (1949). Determination of serum proteins by means of biuret reaction. *Journal of biological chemistry, 177*(2), 751–766.

Herrero, A. M. (2008). Raman spectroscopy for monitoring protein structure in muscle food systems. *Critical Reviews in Food Science & Nutrition, 48*(6), 512–523.

Jantakoson, T., Thavaroj, W., & Konno, K. (2013). Myosin and actin denaturation in frozen stored kuruma prawn *Marsupenaeus japonicus* myofibrils. *Fisheries Science, 79*(2), 341–347.

Ko, W. C., Shi, H. Z., Chang, C. K., Huang, Y. H., Chen, Y. A., & Hsieh, C. W. (2016). Effect of adjustable parallel high voltage on biochemical indicators and actomyosin Ca^{2+}-ATPase from tilapia (*Oreochromis niloticus*). *LWT - Food Science and Technology, 69*, 417–423.

Koch, L., Emin, M. A., & Schuchmann, H. P. (2017). Reaction behaviour of highly concentrated whey protein isolate under defined heat treatments. *International Dairy Journal, 71*, 114–121.

Kong, C. H. Z., Hamid, N., Liu, T., & Sarojini, V. (2016). Effect of antifreeze peptide pretreatment on ice crystal size, drip loss, texture, and volatile compounds of frozen carrots. *Journal of Agricultural & Food Chemistry, 64*(21), 4327–4336.

Kong, C. H. Z., Hamid, N., Ma, Q., Lu, J., Wang, B. G., & Sarojini, V. (2017). Antifreeze peptide pretreatment minimizes freeze-thaw damage to cherries: an in-depth investigation. *LWT - Food Science and Technology, 84*, 1–29.

Langevin, D. (2014). Surface shear rheology of monolayers at the surface of water. *Advances in Colloid & Interface Science, 207*(1), 121–130.

Liang, Y. Y., & Zhang, L. M. (2007). Bioconjugation of papain on superparamagnetic nanoparticles decorated with carboxymethylated chitosan. *Biomacromolecules, 8*(5), 1480–1486.

Liu, Q., Lu, Y., Han, J. C., Chen, Q., & Kong, B. H. (2015). Structure-modification by moderate oxidation in hydroxyl radical-generating systems promote the emulsifying properties of soy protein isolate. *Food Structure, 6*, 21–28.

Lu, H., Zhang, L. T., Li, Q. Z., & Luo, Y. K. (2017). Comparison of gel properties and biochemical characteristics of myofibrillar protein from bighead carp (*Aristichthys nobilis*) affected by frozen storage and a hydroxyl radical-generation oxidizing system. *Food Chemistry, 223*, 96–103.

Lv, M., Mei, K., Zhang, H., Xu, D., & Yang, W. (2018). Effects of electron beam irradiation on the biochemical properties and structure of myofibrillar protein from Tegillarca granosa, meat. *Food Chemistry, 254*, 64–69.

Manuchehrabadi, N., Zhe, G., Zhang, J. J., Ring, H. L., Shao, Q., Liu, F., McDermott, M., Fok, A., Rabin, Y., Brockbank, K. G. M., Garwood, M., Haynes, C. L., & Bischof, J. C. (2017). Improved tissue cryopreservation using inductive heating of magnetic nanoparticles [J]. *Science Translational Medicine, 9*(379), eaah4586–eaah4597.

Hernández-Martínez, M., Gallardo-Velázquez, T., Osorio-Revilla, G., Almaraz-Abarca, N., & Castañeda-Pérez, E. (2014). Application of MIR-FTIR spectroscopy and chemometrics to the rapid prediction of fish fillet quality. *CyTA - Journal of Food, 12*(4), 369–377.

Mao, W. J., Li, X. L., Fukuoka, M., Liu, S. C., Ji, H. W., & Sakai, N. (2016). Study of Ca^{2+}-ATPase activity and solubility in the whole kuruma prawn (*Marsupenaeus japonicus*) meat during heating: based on the kinetics analysis of myofibril protein thermal denaturation. *Food and Bioprocess Technology, 9*(9), 1511–1520.

Mehta, N. K., & Nayak, B. B. (2017). Bio-chemical composition, functional and rheological properties of fresh meat from fish, squid and shrimp: a comparative study. *International Journal of Food Properties.*

Nielsen, M. K., & Jørgensen, B. M. (2004). Quantitative relationship between trimethylamine oxide aldolase activity and formaldehyde accumulation in white muscle from gadiform fish during frozen storage. Journal of Agricultural & Food Chemistry, 52(12), 3814–3822

Ohta, F., & Yamada, T. (2011). On the correlation between the concentrations of phosphates and chlorides in the unfrozen portions of the frozen fish muscle juices and the denaturation rate of fish muscle protein during frozen-storage. *Transactions of the Japan Society of Refrigerating & Air Conditioning Engineers, 7*(09), 1893–1898.

Peng, B., Li, Y. Q., Ding, S. Y., & Yang, J. (2017). Characterization of textural, rheological, thermal, microstructural, and water mobility in wheat flour dough and bread affected by trehalose. *Food Chemistry, 233*, 369–377.

Shi, Y., Li, R. Y., Tu, Z. C., Ma, D., Wang, H., & Huang, X. Q. (2015). Effect of γ-irradiation on the physicochemical properties and structure of fish myofibrillar proteins. *Radiation Physics and Chemistry, 109*(10), 70–72.

Sun, W. Z., Zhao, Q. Z., Zhao, M. M., Yang, B., Cui, C., & Ren, J. Y. (2011). Structural evaluation of myofibrillar proteins during processing of Cantonese sausage by Raman spectroscopy. *Journal of Agricultural & Food Chemistry, 59*(20), 11070–11077.

Sun, X. D., & Arntfield, S. D. (2012). Gelation properties of chicken myofibrillar protein induced by transglutaminase crosslinking. *Journal of Food Engineering, 107*(2), 226–233.

Wong, B. T., Li, D., & Augustin, M. A. (2011). Deamidated wheat protein-dextran Maillard conjugates: effect of size and location of polysaccharide conjugated on steric stabilization of emulsions at acidic pH. *Food Hydrocolloids, 25*(6), 1424–1432.

Xia, X., Kong, B., Liu, Q., & Liu, J. (2009). Physicochemical change and protein oxidation in porcine longissimus dorsi as influenced by different freeze-thaw cycles. *Meat Science, 83*(2), 239–245.

Xiong, G., Han, M., Kang, Z., Zhao, Y., Xu, X., & Zhu, Y. (2016). Evaluation of protein structural changes and water mobility in chicken liver paste batters prepared with plant oil substituting pork backfat combined with pre-emulsification. *Food Chemistry, 196*, 388–395.

Yeh, C. M., Kao, B. Y., & Peng, H. J. (2009). Production of a recombinant type 1 antifreeze protein analogue by L. lactis and its applications on frozen meat and frozen dough. *Journal of Agricultural & Food Chemistry, 57*(14), 6216–6223.

Zhang, T., Li, Z. J., Wang, Y. M., Xue, Y., & Xue, C. H. (2016). Effects of konjac glucomannan on heat-induced changes of physicochemical and structural properties of surimi gels. *Food Research International, 83*, 152–161.

Zhang, T., Xue, Y., Li, Z., Wang, Y., Yang, W., & Xue, C. (2015). Effects of ozone-induced oxidation on the physicochemical properties of myofibrillar proteins recovered from bighead carp (*Hypophthalmichthys nobilis*). *Food and Bioprocess Technology, 8*(1), 181–190.